electronics

MDPI

Article

Quality Mapping of Offset Lithographic Printed Antenna Substrates and Electrodes by Millimeter-Wave Imaging

Jiao Zhang [1], Jianhua Tang [2], Wenfeng Sun [1,*], Yan Zhang [1], Xinke Wang [1] and Bin Yang [2,*]

[1] Department of Physics, Beijing Key Laboratory for Metamaterials and Devices, Beijing Advanced Innovation Center for Imaging Theory and Technology, Capital Normal University, Beijing 100048, China; zhangjiaogx@163.com (J.Z.); yzhang@cnu.edu.cn (Y.Z.); wxk82721@cnu.edu.cn (X.W.)

[2] Faculty of Science and Engineering, University of Chester, Thornton Science Park, Chester CH2 4NU, UK; j.tang@chester.ac.uk

* Correspondence: wfsun@cnu.edu.cn (W.S); b.yang@chester.ac.uk (B.Y.); Tel: 0044-1244512521

Received: 5 June 2019; Accepted: 12 June 2019; Published: date

Abstract: Offset lithographic printed flexible antenna substrate boards and electrodes have attracted much attention recently due to the boost of flexible electronics. Unmanned quality inspection of these printed substrate boards and electrodes demands high-speed, large-scale and nondestructive methods, which is highly desired for manufacturing industries. The work here demonstrates two kinds of millimeter (mm)-wave imaging technologies for the quality (surface uniformity and functionality parameters) inspection of printed silver substrates and electrodes on paper and thin polyethylene film, respectively. One technology is a mm-wave line scanner system and the other is a terahertz-time domain spectroscopy-based charge-coupled device (CCD) imaging system. The former shows the ability of detecting transmitted mm-wave amplitude signals only; its detection is fast in a second time scale and the system shows great potential for the inspection of large-area printed surface uniformity. The latter technology achieves high spatial resolution images of up to hundreds of micrometers at the cost of increased inspection time, in a time scale of tens of seconds. With the exception of absorption rate information, the latter technology offers additional phase information, which can be used to work out 2D permittivity distribution. Moreover, its uniformity is vital for the antenna performance. Additionally, the results demonstrate that compression rolling treatment significantly improves the uniformity of printed silver surfaces and enhances the substrate's permittivity values.

Keywords: millimeter-wave measurement; flexible electronics; quality control; surface uniformity; permittivity distribution

1. Introduction

In recent years, flexible and stretchable electronics based on modern printing technologies have developed at an unprecedented rate and are involved in various applications, such as antennas for wearable wireless communications [1,2] and bio-molecular monitors [3]. At the heart of this technology trend, flexible substrate boards and electrodes are vital components for the design and performance of such antennas. Offset lithographic printing is an established high-volume, high-speed printing technique and it has been developed to pattern a wide range of conductive materials on diverse substrates, such as flexible papers and polymers, to realize low-cost, large-area and multifunctional electronic performances [4–8]. There is no doubt that this printing technology has shown great potential in satisfying both printing speed and quality. However, there are still some

challenges that remain to be solved, including uneven printed surface due to fluidic instability and side effects from post-treatment, such as the formation of unwanted dimensional structures [9,10]. It is essential for manufacturers to track parameter variation of the substrate boards and electrodes such as sheet resistance [11], dielectric permittivity [12,13], surface roughness [14], pin-hole defects [15] and other parameters related to issues of uniformity [16]. However, traditional probe-based electrical measurements, for example using eddy current probes [17], are time-consuming and inefficient, as they are unable to match modern printing speeds. Conventional surface imaging techniques such as atomic force microscopy (AFM), scanning electron microscopy (SEM) and optical microscopy are expensive surface detection tools. Furthermore, they are good at screening small surface areas but lack feasibility for large-scale quality inspection. Recently, millimeter (mm)-wave antenna near-field scanning and terahertz (THz) time domain spectroscopy (TDS)-based characterization methods [18] have been used to probe sintering temperature impact on offset lithographic printed antenna substrate boards. THz-TDS was also implemented by Zhuldybina et al. to check the conductivity of printed electronics by looking at the transmission of vortex phase plate made from V-shape antennas [19]. Millimeter-waves, defined to span frequencies of 30 to 300 GHz (10 to 1 mm in wavelength), affords remarkable natural advantages of electromagnetic waves, which are intrinsically safe, non-ionizing and non-destructive, and are also sensitive to materials' microstructural differences [20] and surface properties [21,22]. Probing transmitted or reflected mm-wave radiation from offset lithographic printed samples can create pinpoint images of large area surface evenness as well as functionally related parameters such as loss and permittivity values. mm-wave and THz imaging techniques have been developed for last 20 years [23]. Security check-out imaging systems at airports is the most successful civil application in recent years [24], though the low-throughput imaging rate still impedes its screening efficiency. To achieve quality inspection with a high speed, on a large scale and with a high volume throughput in printing electronic industries, in this work, antenna line scanning and THz time domain spectroscopy (TDS)-based charge-coupled device (CCD) imaging systems are implemented to monitor the surface uniformity of the printed antenna substrate boards and electrodes, as well as to quantify their functionality, particularly the permittivity and loss properties for antenna design. This work demonstrates the great potential of mm-wave techniques in screening the surface quality (uniformity and functionality) of printed flexible substrate boards and electrodes with large-scale and time-efficient capabilities, which is a currently lacking and highly desirable technology for high-yield printed electronic industries.

2. Materials and Methods

Commercial conductive silver ink was acquired from Thomas Swan and Co. Ltd. (Consett, UK) and it offset lithographically printed by Manroland Sheetfed Offset Presses at Nano Products Co Ltd (West Yorkshire, UK). Two kinds of substrates were used: Teslin style paper and thin polyethylene film. Inspired by the work of Arapov et al. [25], in which rolling compression was used to improve the conductivity of printed binder-based graphene inks, one of the printed silver samples on Teslin style paper substrates was compressed by a mini roller mill at room temperature and the other was not. Photographs of the samples are shown in Figures 1a,b; SEM images of the selected local small area (Leo 1455VP instrument with SmartSEM software v05.03.06, Carl Zeiss AG, Oberkochen, Germany) are shown in Figures 1c,d. From the SEM images, it can be seen that the rolling process enhanced the local silver distribution and made the sample smoother than the non-compressed sample.

For the sample printed on the THz thin transparent polyethylene film substrate, it included different interdigital electrode patterns made by thin (363 μm ± 8 μm width) silver lines and polyethylene intervals (227 μm ± 5 μm width). A photograph and a magnified area are shown in Figures 1e,f; the widths of the silver line and interval were determined by optical microscope (Leica DM2700M, ×10 magnification), as shown in Figure 1g. The thickness of all three samples were measured in micrometers: the uncompressed silver Teslin substrate was 0.216 ± 0.002 mm, the compressed silver Teslin substrate was 0.198 ± 0.002 mm and the silver polyethylene electrode was

0.133 ± 0.001 mm. The thickness uncertainty was based on 10 measurements and the maximum 2 μm thickness variation had negligible influence on the mm-wave signals.

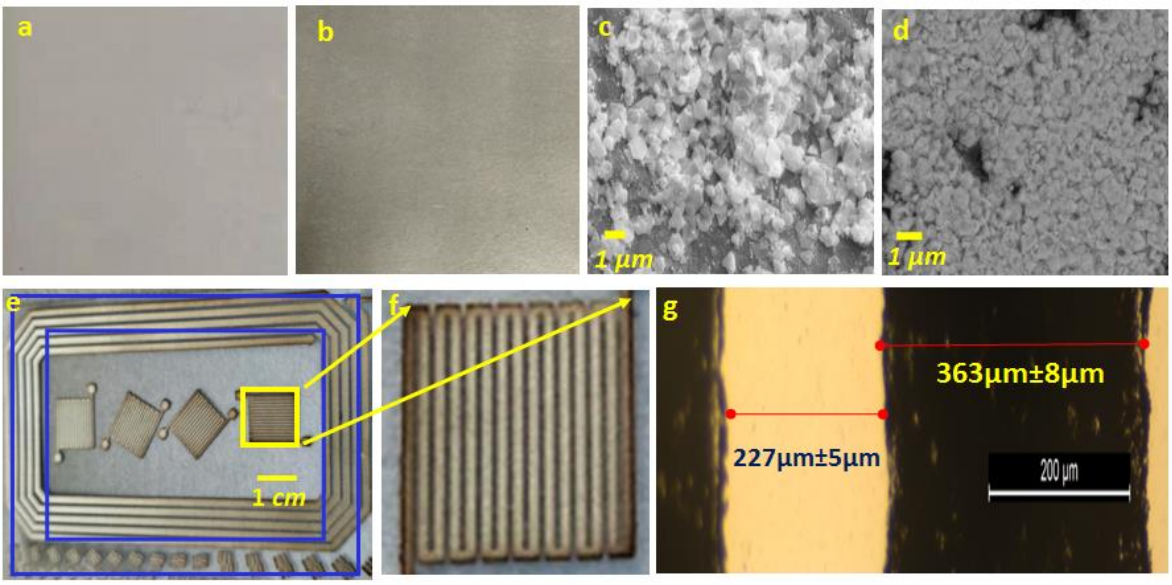

Figure 1. (**a**) Photo of printed silver on a Teslin paper substrate without rolling compression treatment; (**b**) photo of printed silver on a Teslin paper substrate with rolling treatment; (**c**) and (**d**) are SEM images (5000X× magnification) of the small sample areas in (a) and (b). (**e**) Photo of printed silver interdigital pattern electrodes on thin polyethylene film where the blue frame outlines the resin-based sample holder and the gold frame area is magnified and shown in (**f**); (**g**) a randomly selected section of silver lines and polyethylene gap in (f) is further imaged by optical microscopy where the black area presents the silver lines and the yellow-orange area is the polyethylene gaps.

Two mm-wave imaging systems were developed to check printing qualities. The first one is the 100 GHz 2D line scanner system, as shown in Figure 2, where the 100 GHz source is an IMPact ionization Avalanche Transit-Time (IMPATT) diode and the detector is a GaAs HEMT (high electron mobility transistor)-based line scanning array, supplied by Terasense Ltd. The samples under the test are mounted on the side of a 1D slider and the line scanner array is located spatially orthogonally just beneath the slider (less than 1 mm) in order to achieve a 2D near-field imaging system. The slider speed in this work was set at 10 cm per second (the slider's maximum speed limitation), and the samples were mounted on the resin frame as shown in Figure 1e.

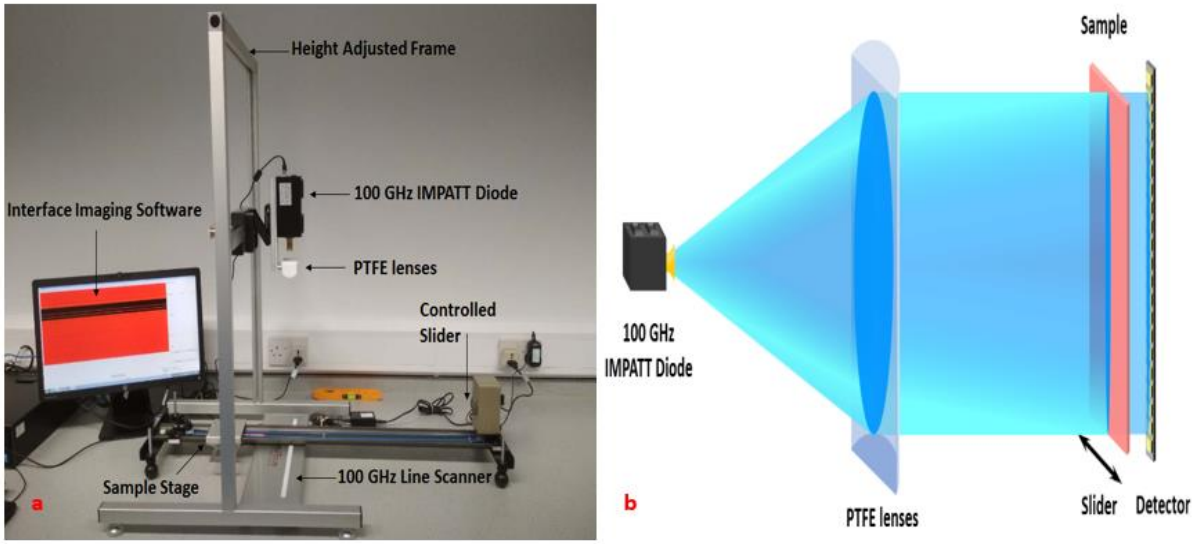

Figure 2. (**a**) Photograph and (**b**) schematic plot of the 100 GHz line scanning imager.

The second experimental system is the THz-TDS transmission-based CCD imager, the schematic plot and photo of which are shown in Figure 3. The core part of the system is exactly that same as a conventional THz-TDS system where the THz signal (from 200 GHz to 3 THz) is generated by an illuminating pump femtosecond laser on ZnTe crystal caused by the light rectification effect and another ZnTe crystal is used as the THz detector, coupling with the same femtosecond probe beam by an electro-optic mechanism. Nevertheless, as an exceptional quasi-near-field imaging system [26], the right side of the ZnTe detector crystal (3 mm thickness, 6 mm diameter circle) is coated with an anti-reflection coating material to ensure that most of the probe light enters the crystal and then is reflected back from the left side of its surface. The samples' mm-wave and THz information is carried by the polarization state of this reflected probe light and then captured by a CCD camera. Based on Blanchard's work on THz near-field microscopy [27], the spatial resolution can reach up to one 30th of the wavelength if the sample is deposited on the detector crystal. Our printed samples were nearly touching the ZnTe electro-optic crystal, with a gap of less than 100 μm.

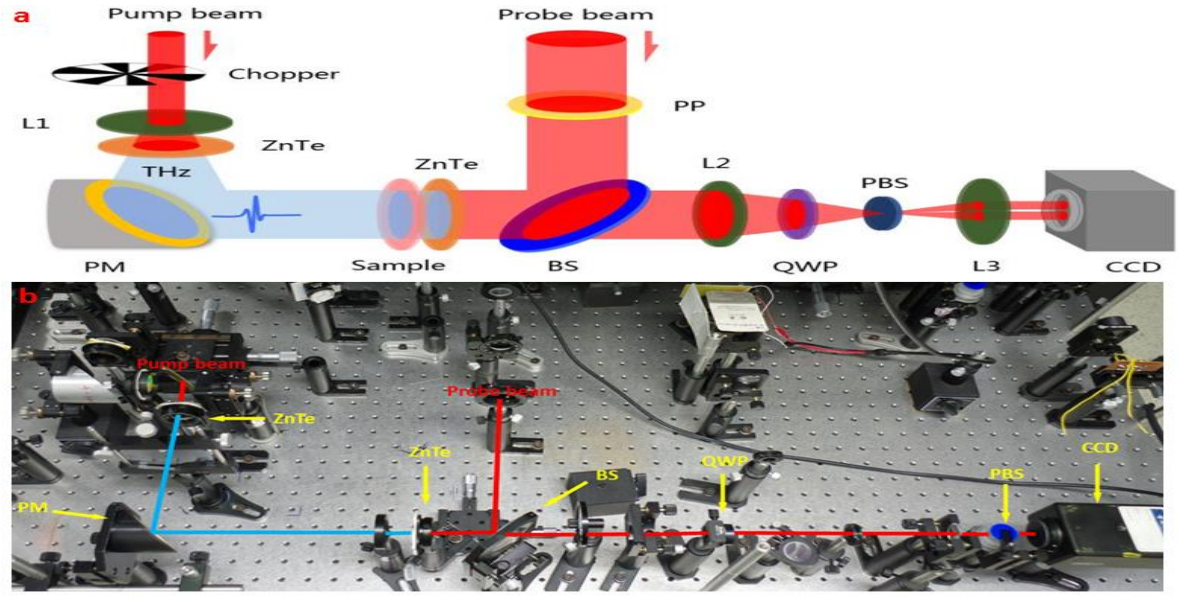

Figure 3. (**a**) Schematic plot and (**b**) photo of the terahertz (THz) time domain spectroscopy (TDS)-based charge-coupled device (CCD) imaging system: pump and probe beams come from a femtosecond laser from Spectra Physics with a center wavelength of 800 nm, a pulse width of 100 fs and a repetition rate of 1 kHz. L1–L3, lenses; PM, parabolic mirror; BS, beam splitter; PP, polarization plate; QWP, quarter-wave plate; PBS, polarization beam splitter; CCD, charge-coupled device.

3. Results and Discussion

The images acquired from the 100 GHz line scanner are shown in Figure 4, where the 33 × 67 pixels cover the area of 5 cm × 10 cm. The GaAs HEMT array detector offers a single pixel of 1.5 mm line width (half wavelength) in both X and Y directions, and the total scanning time is 1 second. The data were calibrated against the empty system, i.e., transmission data between the 100 GHz IMPATT source and detector arrays solely. The sample holder was made from resin, which is a low loss material at mm-wave frequencies; therefore, a rectangular frame (in dark red color) image could be identified with the exception of the area covered by the printed silver. Comparing Figure 4a with Figure 4b, the sliver substrate sample with rolling treatment showed great uniformity (large uniform blue area in Figure 4b) and the rolled silver surface strongly blocked the mm-wave signal; however, the sample without rolling treatment showed many transmitted patches where the mm-wave signals could still propagate through. The results indicate that the rolling treatment significantly improved the uniformity of the printed silver, which can enhance its performance as an antenna substrate. The results agree with the SEM outcomes, as shown in Figures 1c,d. Furthermore, they present a large screening area in a second time scale, which is far more efficient than SEM.

The third sample is based on a thin polyethylene film substrate that includes many interdigital electrode patterns made from thin silver lines (as shown in Figure 1e). This was difficult to image clearly by the line detector with its 1.5 mm spatial resolution limitation. The result in Figure 4c shows some blue color patch areas where highly dense sliver interdigital electrodes strongly blocked and diffracted the mm-wave signals, but the areas with polyethylene film allowed plenty of mm-wave signals to propagate through. As the line scanner system only detects the transmitted amplitude, it is highly advanced in scanning large areas and offers excellent time efficiency.

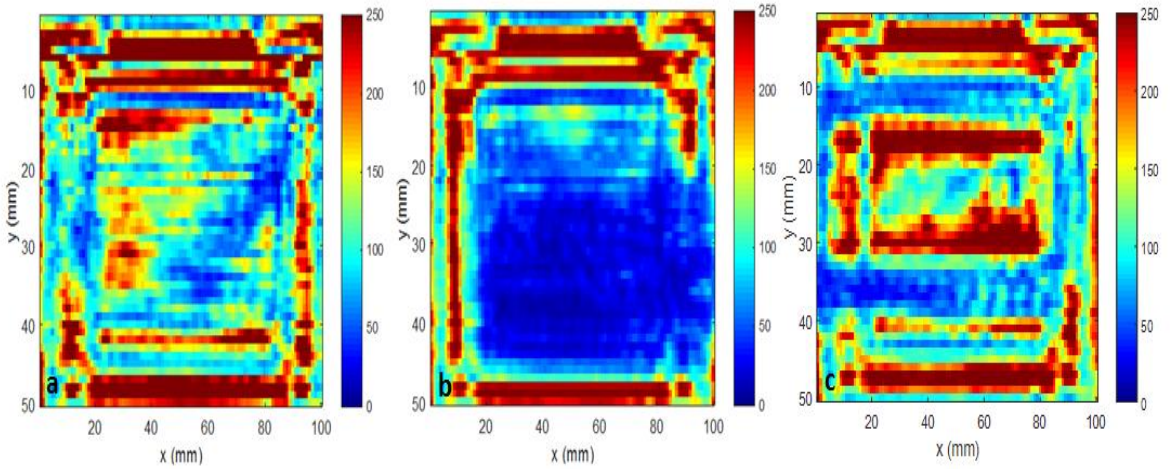

Figure 4. Images of transmitted amplitude information acquired from the mm-wave line scanner imager at 100 GHz: (**a**) printed silver ink on a Teslin paper substrate without rolling compression treatment after printing; (**b**) printed silver ink on Teslin paper substrate with rolling compression treatment after printing; (**c**) printed silver interdigital electrode ink on a thin polyethylene film substrate. The hot red color indicates higher amplitude mm-wave signals transmitted through the samples and the dark blue denotes lower amplitude signals transmitted through the samples.

The THz-TDS-based CCD imaging system can detect both amplitude and phase information due to its unique coherent detection mechanism. However, its scanning area is limited by the size of the ZnTe detector crystal, as it is used to acquire the wave front information of the THz electric field. In our experiments, the inspection area was equal to the crystal size, i.e., a 6 mm diameter circle area. For the sample printed on the paper, a small scanning area was selected, while for the interdigital silver electrode sample, the selected scanning area was photographed as shown in Figure 1f. The acquired mm-wave absorption rate and phase images at 200 GHz are presented in Figure 5, which are shown against the background reference signals, i.e., without printed ink samples in the system. For the compressed paper substrate, the local uniformity was improved. This can be observed from many larger patch-like imaging areas (Figures 5c,d) as well as the increased absorption rate due to the improved surface silver evenness after rolling treatment. Benefiting from quasi-near-field imaging set-up, the CCD-based THz imaging method is able to supply sub-wavelength imaging resolution [26] and the 363 μm wide silver lines can be observed in their mm-wave images as shown in Figures 5e,f, although some diffractions still exist. Comparing the results with those of the line scanner system, the THz-TDS-based CCD imaging system is able to supply additional information of the samples, i.e., the 2D permittivity (ε) distribution of the total effect of printed silver substrates and electrodes. This can be calculated by $\varepsilon = n_s^2 - k_s^2$, where n_s and k_s are the real and imaginary parts of the refractive index of the samples. n_s and k_s can be calculated from the acquired amplitude $E(\omega)$ and phase $\phi(\omega)$ by using Equations (1) and (2) [28,29]

$$n_s(\omega) = 1 + \frac{c}{\omega l}\phi(\omega) \quad (1)$$

$$k_s(\omega) = \frac{c}{\omega l}\left\{\ln|E(\omega)| - \ln\left[\frac{4n_s(\omega)}{(n_s(\omega)+1)^2}\right]\right\} \quad (2)$$

where $E(\omega)$ is the ratio of the received samples' amplitude against the background CCD imaging amplitude and $\phi(\omega)$ is the phase difference between the samples and the background. ω is the angular frequency, c is the speed of light in free space and l the thickness of the samples. The calculated permittivities are shown in Figure 6 and some consistent conclusions are drawn as well—the rolling treatment significantly enhanced local permittivity values; the area with and without thin silver interdigital electrodes showed clear contrast in permittivity values.

For the THz-TDS CCD-based imaging system, there is a balance between the measurement speed and the achieved dynamic range of the system for the CCD-based imaging system. The THz time domain signal is scanned by adjusting the optical path difference between the optical path of the pump beam and the probe beam. Thus, it only takes a few tens of seconds to complete high-quality spectroscopy. Compared with the conventional point-by-point 2D raster scanning system, which needs hours to achieve half wavelength spatial resolution, the CCD-based quasi-near-field imaging system has great time efficiency and spatial resolution. According to our measurements, it takes less than 30 seconds to complete one THz-TDS spectroscopy process; from there the transformed images cover a 6 mm diameter circle area. However, the CCD-based detection system has one technical issue, i.e., poor signal to noise ratio. As the main areas of the samples are covered by conductive silver, the poor signal to noise ratio will significantly destruct the imaging quality, waste the useful wide band THz spectra and cut the validated transmitted signal down to 500 GHz. In this work, the images at 200 GHz were used only to compare the results from the line scanner system and the 363 μm wide sliver lines can be roughly observed at 200 GHz. Certainly, operating multiple scans could significantly increase the signal to noise ratio, which could make the system dynamic range highly competitive in detecting the transmission of printed thin conductive metal samples, albeit with the cost of a longer inspection time. The detailed comparison between these two near-field imaging systems is listed in Table 1.

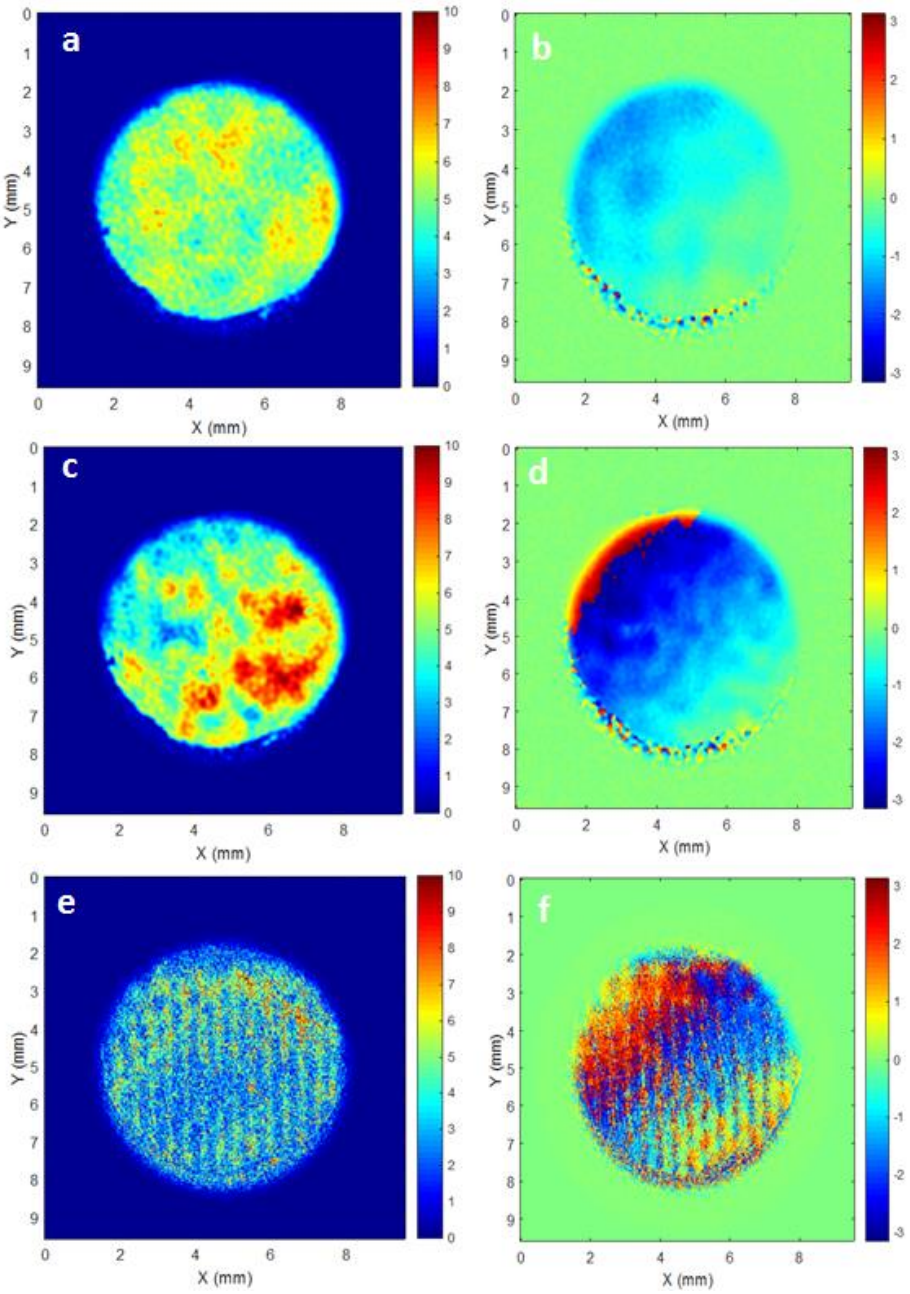

Figure 5. THz-TDS-based CCD imaging results at 200 GHz: (**a**,**b**) printed silver on a Teslin paper substrate without rolling treatment; (**c**,**d**): printed silver on a Teslin paper substrate with rolling treatment; (**e**,**f**) printed silver ink electrodes on a thin polyethylene film substrate. The left plots are the absorption rate (cm^{-1}) and the right plots are the phase angle ($\pi, -\pi$).

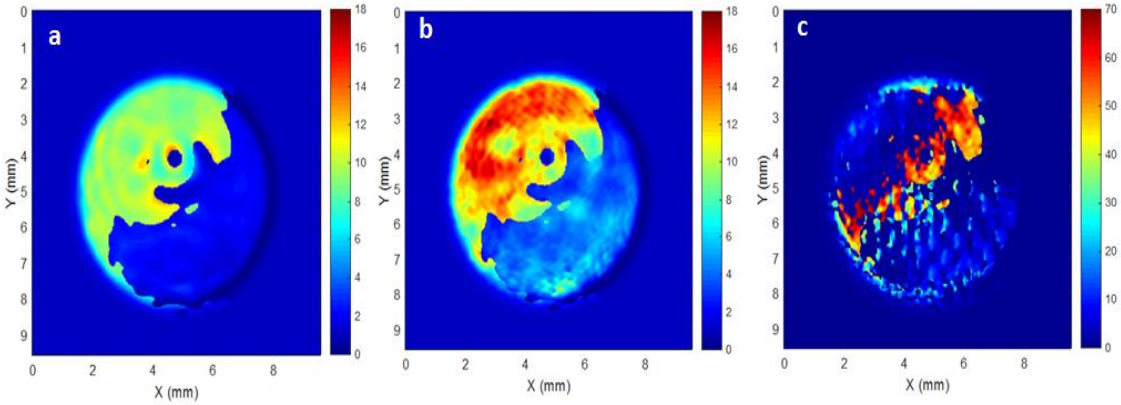

Figure 6. Calculated permittivity of the three samples at 200 GHz: (**a**) printed silver on a Teslin paper substrate without rolling treatment; (**b**) printed silver on a Teslin paper substrate with rolling treatment; (**c**) printed silver ink interdigital electrodes on a thin polyethylene film substrate.

Table 1. Comparison of the two near-field scanning systems: the line scanner imager vs. the THz-TDS CCD imager.

	Line Scanner Imager	**THz-TDS CCD Imager**
Number of Pixels	256 × 1 pixels without moving slider (in this work, 33 × 67 pixels with moving slider)	Dependent on the surface area of the ZnTe detector crystal and CCD camera (187 × 187 pixels in this work)
Pixel size	1.5 × 1.5 mm	32 × 32 μm
Imaging area	384 mm in width; length can be infinite with moving slider	Dependent on the area of the ZnTe detector crystal
Dimension of the system	Source: 12 × 7 × 7 cm Detector: 45.2 × 17.5 × 4.5 cm	Bulk optical system
Detector resolution	1.5 × 1.5 mm^2	32 × 32 μm^2 (CCD camera)
Operating frequency	100 GHz	200 GHz–3 THz
Acquisition rate	1 second	<30 seconds
Interface	Python and Matlab	Labview and Matlab
Advantages	High speed; high throughput and large area inspection; compact system that conveniently integrates with manufacturing line	High spatial resolution; medium speed; acquires both amplitude and phase information
Disadvantages	Limited to mm-wave spatial resolution; only amplitude information-based screening and lack of phase information	Bulk system; screening area is limited by the size of the detector crystal

4. Conclusions

In this study, two quality inspection systems, i.e., a mm-wave IMPATT-HEMT array-based line scanner system and a THz-TDS-based CCD imager, were implemented to inspect the quality (surface uniformity and functionality) of printed antenna substrate boards and electrodes. Both systems showed efficiency in reflecting the contrasted information due to printed surface unevenness. The mm-wave line scanner is capable of large-area and high-throughput inspection by capturing transmitted amplitude signals only, while the THz-TDS-based transmission CCD method showed high spatial resolution up to hundreds of micrometers, albeit at the cost of a longer inspection time. The TDS-based method is able to offer an additional electromagnetic parameter, 2D permittivity distribution, which is an important parameter for high-frequency antenna design. The work presented here on inspecting the impact of rolling treatment drew interesting conclusions; specifically, it was found that compression treatment can significantly improve the local uniformity of the printed surface as well as enhance the effective permittivity of the whole substrate boards. The two mm-wave systems have great potential for applications in high-speed and large-scale quality inspection in printing electronics manufacture industries.

Author Contributions: J.Z. and J.T. implemented the experimental work; B.Y. and W.S. analyzed data and wrote the manuscript; B.Y., W.S., Y.Z. and X.W. revised the manuscript.

Funding: This work was supported in part by the National Natural Science Foundation of China (11474206, 11404224, 1174243, 61675138 and 11774246) and the UK's EPSRC Centre for Innovative Manufacturing in Large Area Electronics (EP/K03099X/1).

Conflicts of Interest: The authors declare no conflict of interest.

References

1. Falade, O.P.; Jilani, S.F.; Ahmed, A.Y.; Wildsmith, T.; Reip, P.; Rajab, K.Z.; Alomainy, A. Design and characterization of a screen-printed millimeter-wave flexible metasurface using copper ink for communication applications. *Flex. Print. Electron.* **2018**, *3*, 045005, doi: https://doi.org/10.1088/2058-8585/aaf0eb.
2. Whittow, W.G.; Chauraya, A.; Vardaxoglou, J.C.; Li, Y.; Torah, R.; Yang, K.; Beeby, S.; Tudor, J. Inkjet-printed microstrip patch antennas realized on textile for wearable applications. *IEEE Antennas Wirel. Propag. Lett.* **2014**, *13*, 71–74.
3. Yang, Y.; Gao, W. Wearable and flexible electronics for continuous molecular monitoring. *Chem. Soc. Rev.* **2018**, doi:10.1039/c7cs00730b.
4. Kumar, V.; Forsberg, S.; Engström, A.-C.; Nurmi, M.; Andres, B.; Dahlström, C.; Toivakka, M. Conductive nanographite–nanocellulose coatings on paper. *Flex. Print. Electron.* **2017**, *2*, 35002.
5. Perelaer, J.; Hendriks, C.E.; Laat, A.W.M.; Schubert, U.S. One-step inkjet printing of conductive silver tracks on polymer substrates. *Nanotechnology* **2009**, *20*, 165303.
6. Rim, Y.S.; Bae, S.-H.; Chen, H.; De Marco, N.; Yang, Y.; Bae, S. Recent Progress in Materials and Devices toward Printable and Flexible Sensors. *Adv. Mater.* **2016**, *28*, 4415–4440.
7. Sowade, E.; Mitra, K.Y.; Ramon, E.; Martínez-Domingo, C.; Villani, F.; Loffredo, F.; Gomes, H.L.; Baumann, R.R. Up-scaling of the manufacturing of all-inkjet-printed organic thin-film transistors: Device performance and manufacturing yield of transistor arrays. *Org. Electron.* **2016**, *30*, 237–246.
8. Khan, S.; Lorenzelli, L.; Dahiya, R.S. Technologies for Printing Sensors and Electronics Over Large Flexible Substrates: A Review. *IEEE Sensors J.* **2015**, *15*, 3164–3185.
9. Chen, S.-P.; Chiu, H.-L.; Wang, P.-H.; Liao, Y.-C. Inkjet printed conductive tracks for printed electronics. *ECS J. Solid State Sci. Technol.* **2015**, *4*, 3026–3033.
10. Sowade, E.; Polomoshnov, M.; Baumann, R.R. The design challenge in printing devices and circuits: Influence of the orientation of print patterns in inkjet-printed electronics. *Org. Electron.* **2016**, *37*, 428–438.
11. Lewis, A.P.; Hunt, C.; Thomas, O.; Wickham, M. High-speed non-contact sheet resistivity monitoring of printed electronics using inductive sensors. *Flex. Print. Electron.* **2017**, *2*, 4, doi: https://doi.org/10.1088/2058-8585/aa9875.
12. Betancourt, D.; Castan, J. Printed antenna on flexible low-cost pet substrate for UHF applications. *PIER C*, **2013,** *38*, 129–140.
13. Beisteiner, C.; Zagar, B.G. Dielectric permittivity measurement of paper substrate using commercial inkjet printers. *Procedia Eng.* **2016**, *168*, 995–998.
14. Altay, B.N.; Jourdan, J.; Turkani, V.S.; Dietsch, H.; Maddipatla, D.; Pekarovicova, A.; Fleming, P.D.; Atashbar, M. Impact of substrate and process on the electrical performance of screen-printed nickel electrodes: fundamental mechanism of ink film roughness. *ACS Appl. Energy Mater.* **2018**, *1*, 7164–7173.
15. Heinrichsdobler, A.; Roigk, J.C.; Schirmeier, F.; Brabec, C.J.; Wehlus, T. Pinhole-free inkjet printing strategies for organic electronics. *Adv. Mater. Technol.* **2017**, *2*, 1700166, doi:https://doi.org/10.1002/admt.201700166.
16. X.Feng, R.Su, T.Happonen, J.Liu and R.Leach, Fast and cost-effective in-process defect inspection for printed electronics based on coherent optical processing. *Optics Express,* ***2018***, vol.26, *11*, 13927–13937.
17. Wang, H.; Kow, J.; Raske, N.; Boer, G.D.; Ghajjari, M.; Hewson, R.; Alazmani, A.; Culmer, P. Robust and high-performance soft inductive tactile sensors based on the Eddy-current effect. *Sens. Actuators, A* **2018**, *271*, 44–52.
18. Zeng, Y.; Edwards, M.; Stevens, R.; Bowen, J.W.; Donnan, R.S.; Yang, B. Terahertz characterisation of UV offset lithographically printed electronic-ink. *Org. Electron.* **2017**, *48*, 382–388.
19. Zhuldybina, M.; Ropagnol, X.; Trudeau, C; Bolduc, M.; Zednik, R.J.; Blanchard, F. Contactless In Situ Electrical Characterization Method of Printed Electronic Devices with Terahertz Spectroscopy. *Sensors* **2019**, *3*, 444.
20. Yu, C.; Zeng, Y.; Yang, B.; Donnan, R.S.; Huang, Z.Xiong, J.; Mahajan, A.; Shi, B.; Ye, H.; Binions, R.; Tarakina, N.V.; Reece, M.J.; Yan, H. Titanium dioxide engineered for near-dispersionless high Terahertz permittivity and ultra-low-loss. *Sci. Rep.* **2017**, *7*, 6639.
21. Schecklman, S.; Zurk, L.M.; Henry, S.; Kniffin, G.P. Terahertz material detection from diffuse surface scattering. *J. Appl. Phys.* **2011**, *109*, 094902.

22. Yang, B.; Donnan, R.S.; Zhou, M.; Kingravi, A.A. Reassessment of the electromagnetic reflection response of human skin at W-band. *Opt. Lett.* **2011**, *36*, 4203–4205.
23. Mittleman, D.M. Twenty years of terahertz imaging. *Opt. Express* **2018**, *26*, 9417.
24. Appleby, R.; Robertson, D.A.; Wikner, D. Millimeter wave imaging: a historical review. In *Proceedings of Volume 10189, Passive and Active Millimeter-Wave Imaging XX, 10189, SPIE Defense + Security, Anaheim, CA, USA, 9–13 April 2017*; Wikner, D.A., Robertson, D.A., Eds; SPIE: Bellingham, WA, USA; Volume 1018902.
25. Arapov, K.; Bex, G.; Hendriks, R.; Rubingh, E.; Abbel, R.; de With G.; Friedrich, H. Conductivity enhancement of Binder-based graphene inks by photonic annealing and subsequent compression rolling. *Adv. Eng. Mater.* **2016**, doi:10.1002/adem.201500646.
26. Wang, X.; Cui, Y.; Hu, D.; Sun, W.; Ye, J.; Zhang, Y. Terahertz quasi-near-field real-time imaging. *Opt. Commun.* **2009**, *282*, 4683–4687.
27. Blanchard, F.; Doi, A.; Tanaka, T.; Hirori, H.; Tanaka, H.; Kadoya, Y.; Tanaka, K. Real-time terahertz near-field microscope. *Opt. Express* **2011**, *19*, 8277–8284.
28. Naftaly, M.; Miles, R.E. Terahertz time-domain spectroscopy for material characterization. *Proc. IEEE* **2007**, *95*, 1658–1665.
29. Scheller, M. Data extraction from Terahertz time domain spectroscopy measurements. *J. Infrared Millimeter Waves* **2014**, *35*, 638–648.